RESEARCH ARTICLE OPEN ACCESS

Quantifying Remyelination Using χ-Separation in White Matter and Cortical Multiple Sclerosis Lesions

Jannis Müller, MD, MSc, Po-Jui Lu, PhD, Alessandro Cagol, MD, Esther Ruberte, PhD, Hyeong-Geol Shin, PhD, Mario Ocampo-Pineda, PhD, Xinjie Chen, MD, Charidimos Tsagkas, MD, PhD, Muhamed Barakovic, PhD, Riccardo Galbusera, MD, Matthias Weigel, PhD, Sabine A. Schaedelin, MSc, Yi Wang, PhD, Thanh D. Nguyen, PhD, Pascal Spincemaille, PhD, Ludwig Kappos, MD, Jens Kuhle, MD, PhD, Jongho Lee, PhD, and Cristina Granziera, MD, PhD

Correspondence
Dr. Granziera
cristina.granziera@usb.ch

Neurology® 2024;103:e209604. doi:10.1212/WNL.0000000000209604

Abstract

Background and Objectives

Myelin and iron play essential roles in remyelination processes of multiple sclerosis (MS) lesions. χ-separation, a novel biophysical model applied to multiecho T2*-data and T2-data, estimates the contribution of myelin and iron to the obtained susceptibility signal. We used this method to investigate myelin and iron levels in lesion and nonlesion brain areas in patients with MS and healthy individuals.

Methods

This prospective MS cohort study included patients with MS fulfilling the McDonald Criteria 2017 and healthy individuals, aged 18 years or older, with no other neurologic comorbidities. Participants underwent MRI at baseline and after 2 years, including multiecho GRE-(T2*) and FAST-(T2) sequences. Using χ-separation, we generated myelin-sensitive and iron-sensitive susceptibility maps. White matter lesions (WMLs), cortical lesions (CLs), surrounding normal-appearing white matter (NAWM), and normal-appearing gray matter were segmented on fluid-attenuated inversion recovery and magnetization-prepared 2 rapid gradient echo images, respectively. Cross-sectional group comparisons used Wilcoxon rank-sum tests, longitudinal analyses applied Wilcoxon signed-rank tests. Associations with clinical outcomes (disease phenotype, age, sex, disease duration, disability measured by Expanded Disability Status Scale [EDSS], neurofilament light chain levels, and T2-lesion number and volume) were assessed using linear regression models.

Results

Of 168 patients with MS (median [interquartile range (IQR)] age 47.0 [21.7] years; 101 women; 6,898 WMLs, 775 CLs) and 103 healthy individuals (age 33.0 [10.5] years, 57 women), 108 and 62 were followed for a median of 2 years, respectively (IQR 0.1; 5,030 WMLs, 485 CLs). At baseline, WMLs had lower myelin (median 0.025 [IQR 0.015] parts per million [ppm]) and iron (0.017 [0.015] ppm) than the corresponding NAWM (myelin 0.030 [0.012]; iron 0.019 [0.011] ppm; both $p < 0.001$). After 2 years, both myelin (0.027 [0.014] ppm) and iron had increased (0.018 [0.015] ppm; both $p < 0.001$). Younger age ($p < 0.001$, $b = -5.111 \times 10^{-5}$), lower disability ($p = 0.04$, $b = -2.352 \times 10^{-5}$), and relapsing-remitting phenotype (RRMS, 0.003 [0.01] vs primary progressive 0.002 [IQR 0.01], $p < 0.001$; vs secondary progressive 0.0004 [IQR 0.01], $p < 0.001$) at baseline were associated with remyelination. Increment of myelin correlated with clinical improvement measured by EDSS ($p = 0.015$, $b = -6.686 \times 10^{-4}$).

RELATED ARTICLE

Editorial
χ-Separation as a Novel MRI Biomarker for Assessing Disease Progression in Multiple Sclerosis: Divide and Conquer
Page e209735

From the Translational Imaging in Neurology (ThINk) Basel (J.M., P.-J.L., A.C., E.R., M.O.-P., X.C., C.T., M.B., R.G., M.W., S.A.S., L.K., C.G.), Department of Biomedical Engineering, Faculty of Medicine, and Neurologic Clinic and Policlinic, MS Center and Research Center for Clinical Neuroimmunology and Neuroscience Basel (RC2NB) (J.M., P.-J.L., A.C., E.R., M.O.-P., X.C., C.T., M.B., R.G., M.W., L.K., J.K., C.G.), University Hospital Basel and University of Basel, Switzerland; Department of Health Sciences (A.C.), University of Genova, Italy; Laboratory for Imaging Science and Technology (H.-G.S., J.L.), Department of Electrical and Computer Engineering, Seoul National University, South Korea; Division of Radiological Physics (M.W.), Department of Radiology, University Hospital Basel; Department of Clinical Research (S.A.S.), Clinical Trial Unit, University Hospital Basel, Switzerland; and Department of Radiology (Y.W., T.D.N., P.S.), Weill Medical College of Cornell University, New York, NY.

Go to Neurology.org/N for full disclosures. Funding information and disclosures deemed relevant by the authors, if any, are provided at the end of the article.

The Article Processing Charge was funded by SNF/University Basel.

Glossary

CLs = cortical lesions; **EDSS** = Expanded Disability Status Scale; **FAST-T2** = fast acquisition with spiral trajectory and adiabatic T2-prep; **FLAIR** = fluid-attenuated inversion recovery; **FSL** = FMRIB software library; **IQR** = interquartile range; **MEGRE** = multiecho gradient echo; **MP2RAGE** = magnetization-prepared 2 rapid gradient echo; **MS** = multiple sclerosis; **MWF** = myelin water fraction; **NAGM** = normal-appearing gray matter; **NAWM** = normal-appearing white matter; **NfL** = neurofilament light chain; **ppm** = parts per million; **PPMS** = primary progressive MS; **QSM** = quantitative susceptibility mapping; **ROI** = region of interest; **RRMS** = relapsing-remitting MS; **SPMS** = secondary progressive MS; **TE** = time to echo; **TI** = inversion time; **TR** = repetition time; **WMLs** = white matter lesions.

Discussion

χ-separation, a novel mathematical model applied to multiecho T2*-images and T2-images shows that young RRMS patients with low disability exhibit higher remyelination capacity, which correlated with clinical disability over a 2-year follow-up.

Introduction

In multiple sclerosis (MS), autoimmune aggression against the CNS myelin sheaths leads to focal demyelination of both white and gray matter.[1] Remyelination, the process of myelin regeneration, may occur as a response to injury, eventually providing metabolic support to the axon, hereby preventing its degeneration.[2] As a consequence, promoting remyelination mechanisms has become a major goal for novel disease-modifying drugs.[2,3]

Iron is essential to myelin production, maintenance, and remyelination processes.[4] It is mostly stored in oligodendrocytes, which are also the main myelin-producing cells in the brain.[4] Postmortem histopathologic and imaging studies showed that—in MS lesions—iron is released from dying oligodendrocytes, causing intracellular and extracellular iron accumulation.[5] Moreover, focal and diffuse iron deposits have been associated with smoldering inflammation and neurodegenerative processes.[6]

Recently, imaging studies using myelin-sensitive PET have demonstrated that remyelination is extremely heterogeneous within lesions and patients.[7] Remyelination was particularly pronounced in patients with lower disability scores[7] and shorter disease duration.[8] Furthermore, the results pointed toward the existence of distinct patient subgroups, some of whom retain a larger remyelination capacity ("good remyelinators") than others ("bad remyelinators").[7] However, PET studies are characterized by complexity, high costs, limited availability, invasiveness, and radiation exposure to patients and are therefore unsuitable for large-scale clinical trials or clinical routine.

Conventional MRI, widely used for brain tissue characterization in clinical settings, lacks specificity for quantifying myelin and iron. Advanced MRI techniques such as quantitative susceptibility mapping (QSM[9,10]), magnetization transfer imaging,[11] diffusion weighted imaging,[12] or T1/T2-relaxometry[13,14] provide more specific estimates of myelin properties[7] but are affected by other components of the brain such as water, axons, or iron deposits. Although iron is a source of contrast for many MRI modalities, the specific quantification of iron is currently challenging.[15] Susceptibility-based MRI measures material magnetization under an external magnetic field.[16] This causes a polarization that can either amplify the magnetic field (known as paramagnetism) or counteract it (diamagnetism).[16,17] QSM determines the bulk susceptibility of a particular tissue through the acquisition of susceptibility-based MRI. However, due to the collective contribution of paramagnetic iron and diamagnetic myelin to the signal, conventional QSM is unable to distinguish a decreased diamagnetic (e.g., demyelination) from an increased paramagnetic component (e.g., iron accumulation). Recently, a new MRI method ("χ-separation" or "chi-separation") has been proposed,[18] which estimates the individual contribution of paramagnetism and diamagnetism to the bulk susceptibility signal. This method has demonstrated the ability to differentiate MS lesions from those resulting from neuromyelitis optica spectrum disorder,[19] but its use in quantitative comparisons with healthy individuals and its potential for detecting longitudinal changes in MS lesions remain uncertain.

In this study, we applied χ-separation in vivo to (1) compare the content of iron and myelin in regions of interest (ROIs) in patients with MS vs healthy individuals, (2) correlate iron and myelin in white matter lesions (WMLs) and cortical lesions (CLs) with clinical disease characteristics, and (3) assess remyelination capacity over time, correlated with clinical changes of disability.

Methods

Study Design, Participants, and Assessment

This study was designed as a cross-sectional and longitudinal analysis of data deriving from a prospective cohort study investigating patients with MS and healthy controls. We included individuals who met the following inclusion criteria:

(1) age of 18 years or older, (2) ability to give informed consent, and for patients (3) MS according to the McDonald Criteria 2017.[20] Participants with psychiatric or neurologic comorbidities other than headache, contraindications for MRI, or pregnant women were excluded. MR images were acquired between October 2018 and December 2022. Participants underwent clinical assessments and imaging at baseline and after follow-up of 2 years. Serum neurofilament light chain (NfL) concentrations were measured at baseline through ultra-sensitive Single-Molecule Array assay at the University Hospital Basel.[21] Disability was quantified by board-certified neurologists and/or certified raters applying the Expanded Disability Status Scale (EDSS). Written informed consent was obtained from all participants. The study protocol was approved by the local ethics committee.

Tissue of Interest

We described iron and myelin in (1) WMLs and their perilesional normal appearing white matter (NAWM), and (2) CLs and their perilesional normal appearing gray matter (NAGM). In addition, to accommodate the absence of comparable lesional tissue in healthy individuals, we assessed (3) the putamen (as a referential ROI with an expected high content of iron[22]), and (4) the corpus callosum (as a referential ROI with an expected high content of myelin[23]) in both patients and healthy individuals. In all tissues of interest, a high diamagnetic susceptibility value on negative susceptibility maps was used as an indicator of high myelin (in the following referred to as "content of myelin"). A high paramagnetic susceptibility value on positive susceptibility maps was interpreted as sign of high iron (likewise referred to as "content of iron").[18]

MRI Acquisition, Reconstruction, and Analysis

Image Acquisition

MR images were acquired on a 3 Tesla Siemens MAGNETOM Prisma scanner. The acquisition protocol included: (1) 3D magnetization-prepared 2 rapid gradient echo[24] (MP2RAGE, Figure 1A; repetition time [TR]/time to echo [TE]/inversion time [TI] 5,000/2.98/700, 2,500 milliseconds, voxel size 1 × 1 × 1 mm), (2) 3D fluid-attenuated inversion recovery (FLAIR, TR/TE/TI = 5,000/386/1,800 milliseconds, voxel size 1 × 1 × 1 mm), (3) fast acquisition with spiral trajectory and adiabatic T2-prep[25] (FAST-T2; spiral TR/TE = 7.5/0.5 milliseconds, 6 T2prep times = 0, 7.5, 17.5, 67.5, 147.5, and 307.5 milliseconds, voxel size 1.25 × 1.25 × 5 mm), and (4) multiecho gradient echo images (MEGRE, TR 49 milliseconds, 10 echoes with TEs = 6.7, 10.8, 14.8, 18.9, 22.9, 27.0, 31.1, 35.1, 39.2, and 43.2 milliseconds, voxel size 0.95 × 0.75 × 3 mm). Additional acquisition details are provided in eTables 1–4.

Figure 1 MRIs and χ-Separation Maps

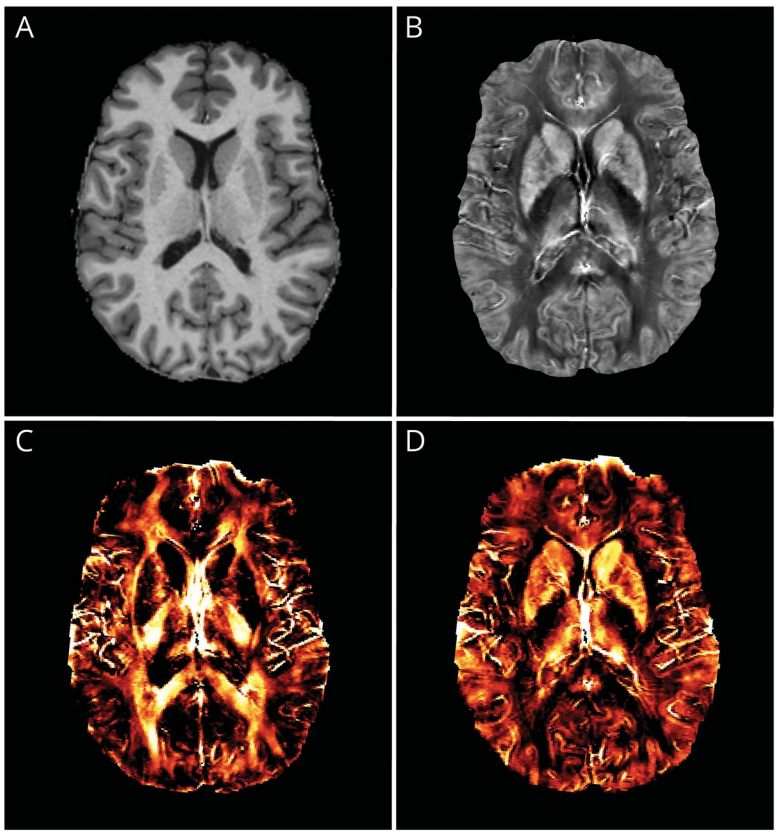

(A) 3D magnetization-prepared 2 rapid gradient echo. (B) Quantitative susceptibility mapping based on multiecho gradient echo. (C) χ-separation map of diamagnetic sources. Brighter tones of yellow indicate higher values of susceptibility (i.e., higher content of myelin). (D) χ-separation map of paramagnetic sources. Brighter tones of yellow indicate higher values of susceptibility (i.e., higher content of iron).

Reconstruction of χ-Separation Maps

To obtain voxel-wise diamagnetic (i.e., myelin-sensitive, Figure 1C) and paramagnetic susceptibility maps (i.e., iron-sensitive, Figure 1D), we applied the χ-separation algorithm, as previously described.[18] Shortly, FAST-T2 images were patient-wise transformed to the MEGRE space. Subsequently, the frequency shift was calculated by sequentially processing the phase images of MEGRE in the order of SEGUE phase unwrapping,[26] V-SHARP background removal,[27] and signal-to-noise ratio-weighted echo combination. T2 and T2* values were estimated by voxel-wise fitting of an exponential function to the multiecho magnitude signal of MEGRE or FAST-T2, respectively. This approach has been validated on both ex vivo and in vivo materials to generate high-quality images of iron and myelin, enabling us to identify histologic details in the brain that are not visible on conventional MR images.[18]

Tissue Segmentation

Referential ROIs (putamen, corpus callosum) were extracted from FreeSurfer using the Desikan-Killiany atlas, after applying the *lesion_filling* command in FMRIB software library (FSL)[28] to avoid tissue misclassification due to WMLs. WMLs were segmented automatically using a deep learning algorithm applied to FLAIR and MP2RAGE images,[29] followed by inspection and manual correction, if needed. To avoid partial volume effects, we excluded WMLs ≤10 voxels on χ-separation maps (equivalent to 16.875 mm^3).[30] To identify the perilesional NAWM, an in-house algorithm automatically identified a 2-voxel layer surrounding each WML. In case of an overlap of 2 NAWM regions (n = 2,837/6,898, mostly 2–3 voxels, maximum 99 overlapping voxels), the susceptibility values were equally distributed between the 2 regions. Experienced raters manually segmented CLs and a 2-voxel layer of adjacent NAGM (avoiding inclusion of WM or CSF) on MP2RAGE images. CLs ≤2 voxels on χ-separation maps (equivalent to 3.375 mm^3) were excluded.[31]

Image Transformation and Coregistration

Images of the same acquisition were rigidly coregistered in the MP2RAGE space using the *flirt* command in FSL (Figure 2). For longitudinal coregistration, skull-stripped MP2RAGE images from baseline and follow-up were affinely registered, followed by nonlinear registration with the MP2RAGE images containing the skull, using the *greedy* diffeomorphic registration algorithm in ITK-Snap.[32,33] To create χ-separation maps, T2 spiral images were aligned with MEGRE images by combining transformation matrices from T2 spiral to MP2RAGE space and then to MEGRE space. Baseline masks for WMLs and CLs were patient-wise transformed to both baseline and follow-up χ-separation spaces, using a sequence of transformation matrices and displacement fields, with 1-time nearest neighbor interpolation applied as a final step. To account for potential lesion expansion at follow-up, we restricted voxels of the NAWM at follow-up to those delineated in the FreeSurfer NAWM maps. Baseline and follow-up ROI masks were transformed to the MEGRE spaces of the respective acquisitions, using transformation matrices from the space of MP2RAGE to the respective MEGRE space. All outputs were manually inspected and corrected if needed, using ITK-SNAP[33] or 3D Slicer (version 4.6.2). For more details of the postprocessing pipeline, see eMethods.

To describe the content of myelin and iron in each ROI/lesion, we used the mean susceptibility value of all voxels contained in each ROI/lesion (*absolute* content of myelin and iron, respectively). In addition, we calculated the *susceptibility index* for myelin and iron separately, as the ratio of the susceptibility value in each lesion, divided by the susceptibility value in the perilesional area (i.e., susceptibility [WMLs]/susceptibility [NAWM] and susceptibility [CLs]/susceptibility [NAGM], respectively. A *susceptibility index* of 1 would indicate an equal susceptibility effect and imply an equal content of myelin or iron, respectively, in a lesion and its perilesional tissue). For clinical correlations, the median susceptibility value of all lesions in each single patient was considered. For longitudinal analyses, the delta between baseline and follow-up of myelin and iron was calculated for each lesion (e.g., for myelin: negative susceptibility [timepoint2] – negative susceptibility [timepoint1]).

Statistical Analysis

We tested the following null hypotheses: (1) there is no difference between susceptibility values on myelin-sensitive or iron-sensitive maps in referential ROIs (putamen and corpus callosum) between patients with MS and healthy individuals, both at baseline and follow-up; (2) there is no difference between susceptibility values on myelin-sensitive or iron-sensitive maps between the tissues of interest (WMLs, CLs, NAWM, NAGM, putamen, and corpus callosum) in patients with MS; (3) the correlation coefficient of the susceptibility index in WMLs or CLs, and demographic (age, sex) or clinical characteristics (disease phenotype, disease duration, EDSS, T2-lesion number and volume, CLs, and NfL) is 0; (4) the difference of susceptibility values of WMLs and CLs on myelin-sensitive or iron-sensitive maps between baseline and follow-up is 0; and (5) the correlation coefficient of the changes between baseline and follow-up, and the demographic or clinical characteristics is 0. To test these hypotheses, we used Wilcoxon rank-sum tests for unpaired comparisons, and Wilcoxon signed rank tests for paired comparisons, followed by Bonferroni correction to adjust for multiple comparisons. For the longitudinal comparisons of lesions (i.e., baseline vs follow-up), we additionally applied linear mixed models using patients as a random intercept to adjust for the higher age of patients at follow-up. To describe correlation coefficients β, we used univariable and multivariable linear regression models. To classify individuals as "top improver" or "top progressor," we identified the 5% of patients exhibiting the most substantial EDSS change between baseline and follow-up in both positive and negative directions, respectively. In case that more than 5% exhibited the same EDSS change, we included all patients with the considered EDSS change to the respective group. In an exploratory analysis, we estimated the heterogeneity of (re-)

Figure 2 Imaging Postprocessing and Transformation Pipeline

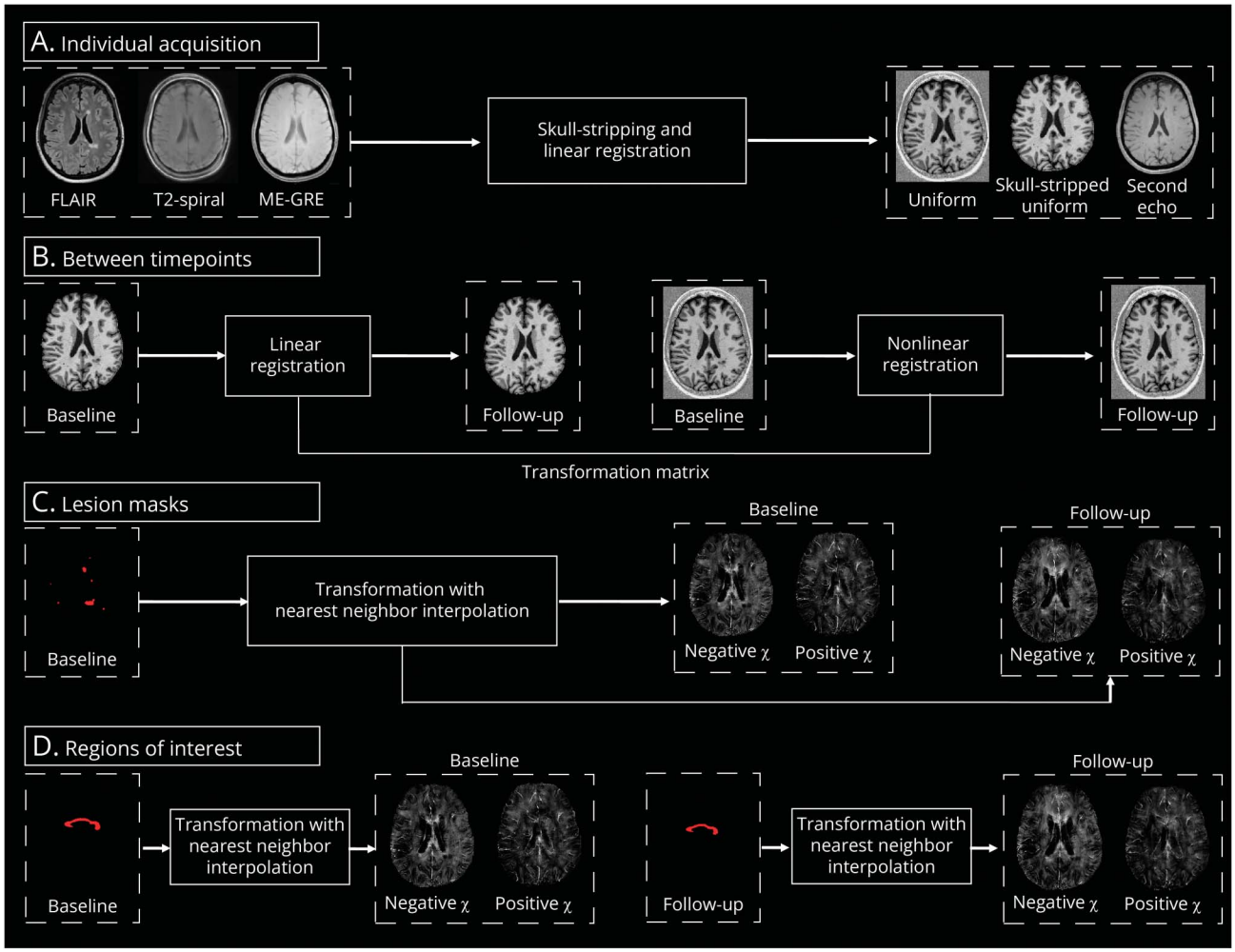

(A) Individual acquisitions were skull stripped and rigidly coregistered using FSL. (B) Longitudinal acquisitions were coregistered on MP2RAGE, as follows: MP2RAGE were first affinely (skull-stripped) and then nonlinearly (with the skull) registered using ITK Snap (greedy diffeomorphic registration). (C) Lesion masks (i.e., masks for white matter lesions, cortical lesions, normal appearing white matter, and normal appearing gray matter) from baseline were transformed to baseline and follow-up maps, using nearest neighbor interpolation. (D) Regions of interest (i.e., masks for corpus callosum and putamen derived from FreeSurfer) were transformed from baseline to baseline and from follow-up to follow-up, respectively, using nearest neighbor interpolation. FLAIR = fluid-attenuated inversion recovery; FSL = FMRIB software library; MEGRE = multiecho gradient echo; MP2RAGE = magnetization-prepared 2 rapid gradient echo; χ = chi (indicates negative and positive χ-separation maps).

myelination within lesions, by comparing susceptibility standard deviations in lesions.

Statistical analysis was performed using R studio.[34] Normally distributed variables are given as mean ± SD, nonnormally distributed variables as median and interquartile range (IQR). A $p < 0.05$ was considered statistically significant.

Data Availability

Data generated or analyzed during the study are available from the corresponding author on reasonable request.

Results

Cohort Description

Demographic and clinical characteristics of the 168 patients and 103 healthy individuals are given in Table 1. The MS cohort was mostly composed of female (60%) patients, with a median age of 47.0 years (IQR 21.7), median EDSS of 3.0 (IQR 3), and median disease duration of 6.2 years (IQR 16.3). Relapsing-remitting MS (RRMS) disease course was the most prevalent clinical MS phenotype (n = 98 [58.3%]), followed by secondary progressive (SPMS, n = 46 [27.7%]) and primary progressive MS (PPMS, n = 24 [14.3%], eTable 5). Healthy individuals were considerably younger (median [IQR] age 33 [10.5] years) but exhibited a similar proportion of women (57/103, 58.7%).

In total, we analyzed 6,898 WMLs and 775 CLs at baseline (median WMLs per patient: 34.5 [IQR 39.5]; median CLs per patient: 2 [IQR 9]; median volume WMLs: 45.56 mm^3 [IQR 45.56]; CLs 15.19 mm^3 [IQR 15.45]). Follow-up was performed in 108 of 168 (64.3%) patients after a median of 2.0 years (IQR 0.1), allowing us to longitudinally analyze 5,030

WMLs and their corresponding NAWM, as well as 485 CLs and their corresponding NAGM. In healthy individuals, 62 of 103 (63.9%) were followed up after 2.0 years (IQR 0.1).

Cross-Sectional Study of Iron and Myelin in Referential Regions of Healthy Individuals vs Patients With MS

On myelin-sensitive maps, there was a lower median susceptibility value in the corpus callosum of patients with MS vs healthy individuals (median [IQR] 0.043 [0.01] vs 0.044 [0.009] parts per million [ppm], p = 0.047, Wilcoxon rank-sum test, Figure 3A); however, this did not withstand the adjustment for multiple comparisons. The content of myelin in the putamen was similar, at both baseline and follow-up.

The putamen of patients with MS showed higher susceptibility values on iron-sensitive maps than healthy individuals, but this finding lost statistical significance after adjustment for age (linear regression model). The content of iron in the corpus callosum was comparable between healthy individuals and patients.

Cross-Sectional Study of Iron and Myelin in White Matter Lesions, Cortical Lesions, and Regions of Interest in Patients With MS

Comparison of Tissues

In patients with MS, the *absolute* susceptibility values on myelin-sensitive and iron-sensitive maps varied significantly among the tissues of interest (Figure 4), indicating the highest content of myelin in the corpus callosum (median 0.043, IQR 0.010 ppm) and the highest content of iron in the putamen (median 0.053, IQR 0.023 ppm).

In WMLs, the *absolute* susceptibility values suggested lower myelin than in the corresponding NAWM (median 0.025 [IQR 0.015] vs 0.030 [0.012] ppm, $p < 0.001$, Wilcoxon rank-

Table 1 Demographics and Clinical Characteristics of Patients

	Patients (N = 168)	Controls (N = 103)
Age, y, median (IQR)	47.0 (21.7)	33.0 (10.5)
Sex, female, n (%)	101 (60.1)	57 (58.7)
Disease course, n (%)		
RRMS	98 (58.3)	n.a.
SPMS	46 (27.4)	
PPMS	24 (14.3)	
EDSS at baseline, median (IQR)	3.0 (3)	n.a.
Patients with a follow-up, n (% of all patients)	108 (64.3)	62 (63.9)
Timepoint of follow-up MRI, y, median (IQR)	2.0 (0.1)	2.0 (0.1)
EDSS at follow-up, median (IQR)	3.0 (3.75)	n.a.
Disease duration at baseline, y, median (IQR)	6.2 (16.3)	n.a.
No. of T2-hyperintense white matter lesions, median (IQR)	43 (51.25)	n.a.
Volume of T2-hyperintense white matter lesions, mm^3, median (IQR)	45.56 (86.06)	n.a.
No. of T1-hyperintense cortical lesions, median (IQR)	2 (9.0)	n.a.
Volume of T1-hyperintense cortical lesions, mm^3, median (IQR)	15.19 (16.45)	n.a.
Serum NfL, median (IQR)	8.4 (5.9)	n.a.
DMT, n (%)		
No DMT	30 (17.8)	n.a.
First-generation injectables	6 (3.6)	
Orals	41 (24.4)	
High effective DMT	91 (54.2)	

Abbreviations: DMT = disease-modifying therapy; EDSS = Expanded Disability Status Scale; IQR = interquartile range; n.a. = not applicable; NfL = neurofilament light chain; PPMS = primary progressive multiple sclerosis; RRMS = relapsing-remitting multiple sclerosis; SPMS = secondary progressive multiple sclerosis. First-generation injectables include interferon β-1a, interferon β-1b, and glatiramer acetate. Orals include fingolimod (n = 16), dimethyl fumarate (n = 15), teriflunomide (n = 2), and siponimod (n = 2). High effective DMTs include ocrelizumab (n = 70), rituximab (n = 16), and natalizumab (n = 4).

Figure 3 Iron and Myelin in the Referential Regions of Interest of Healthy Individuals and Patients With MS at Baseline and Follow-Up

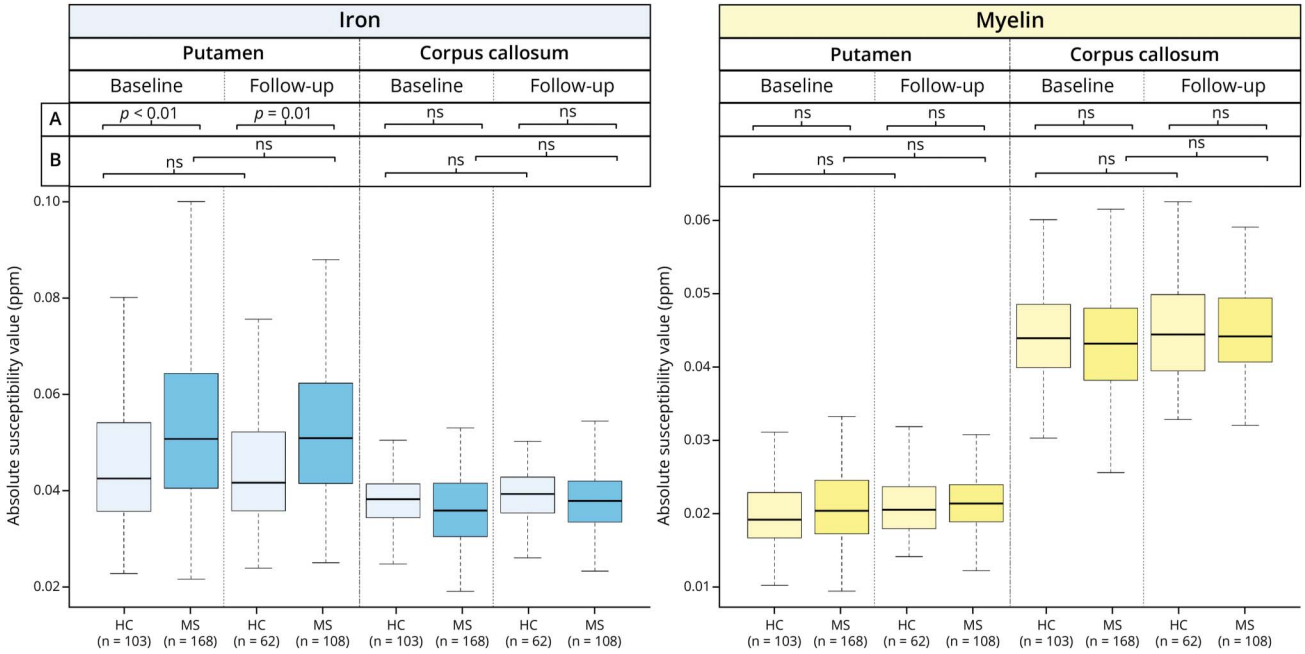

Comparison of *absolute* susceptibility values, in (A) healthy individuals vs patients with MS, and (B) baseline vs follow-up. *p* Values derive from Wilcoxon rank-sum tests and are considered significant if $p < 0.0125$ (i.e., after Bonferroni correction for 4 comparisons). HC = healthy controls; MS = multiple sclerosis; ns = not significant; ppm = parts per million.

sum test). The same was observed for the *absolute* values of iron (median 0.017 [IQR 0.015] vs 0.019 [0.011] ppm, $p < 0.001$, Wilcoxon rank-sum test). In CLs, myelin was comparable with the NAGM, but iron was lower than in the corresponding NAGM (median 0.016 [IQR 0.018], vs 0.022 [0.018] ppm, $p < 0.001$, Wilcoxon rank-sum test). An exploratory analysis of myelin heterogeneity within lesions and patients is given in eFigure 1.

Correlation Between Iron/Myelin Content and Clinical Characteristics

In WMLs, the myelin *susceptibility index* (describing the susceptibility of myelin in lesions, relative to the susceptibility of myelin in the surrounding NAWM) did not show any linear correlation with age. Still, to adjust for residual bias,[35] we adjusted all following models for age. We did not see any association between the myelin *susceptibility index* and sex, disease phenotype or duration, EDSS, T2-lesion number or volume, or CLs number (univariable linear regression models, adjusted for age, see eFigures 2–4).

Considering the iron *susceptibility index* in WMLs, we found higher indices in younger patients ($p < 0.001$, $b = -4.19 \times 10^{-3}$, $aR^2 = 0.218$, linear regression model) and in patients with lower T2-lesion number ($p = 0.02$, $b = -4.80 \times 10^{-4}$, $aR^2 = 0.2$) and volume ($p = 0.05$, $b = -1.42 \times 10^{-6}$, $aR^2 = 0.23$, univariable linear models, adjusted for age). Otherwise, there were no correlations with the investigated disease characteristic (univariable linear regression models, adjusted for age).

For CLs, no associations between the *susceptibility index* of either iron or myelin and any clinical disease characteristic mentioned above were found.

Longitudinal Study of Iron and Myelin in Referential Regions of Healthy Individuals

Between baseline and follow-up, there were no dynamic changes of iron and myelin, respectively, in both corpus callosum and putamen (Figure 3B).

Longitudinal Study of Iron and Myelin in Patients With MS

After the follow-up of 2 years (IQR 0.1), 48 patients had an unchanged, 47 an increased (median deterioration: 1.0 EDSS step), and 13 an improved EDSS (median improvement: 1.0 EDSS step).

In WMLs, the median *absolute* content of both myelin and iron increased during follow-up (myelin: baseline median 0.025 [IQR 0.014], follow-up 0.027 [IQR 0.014] ppm, $p < 0.001$ in both Wilcoxon signed rank test and linear mixed model adjusted for age; iron: 0.0170 [IQR 0.015], 0.0177 [IQR 0.015] ppm, $p = 0.001$ in Wilcoxon signed-rank test, and $p = 0.03$ in linear mixed model adjusted for age). The same was observed for the *susceptibility index* of myelin (baseline median 0.865 [IQR 0.27], follow-up median 0.882 [IQR 0.253], $p < 0.001$ in both Wilcoxon signed-rank test and linear mixed model adjusted for age) and the *susceptibility index* for iron (baseline median 0.886 [IQR 0.41], follow-up 0.900

Figure 4 Content of Iron (Blue) and Myelin (Yellow) in Regions of Interest in Patients With MS

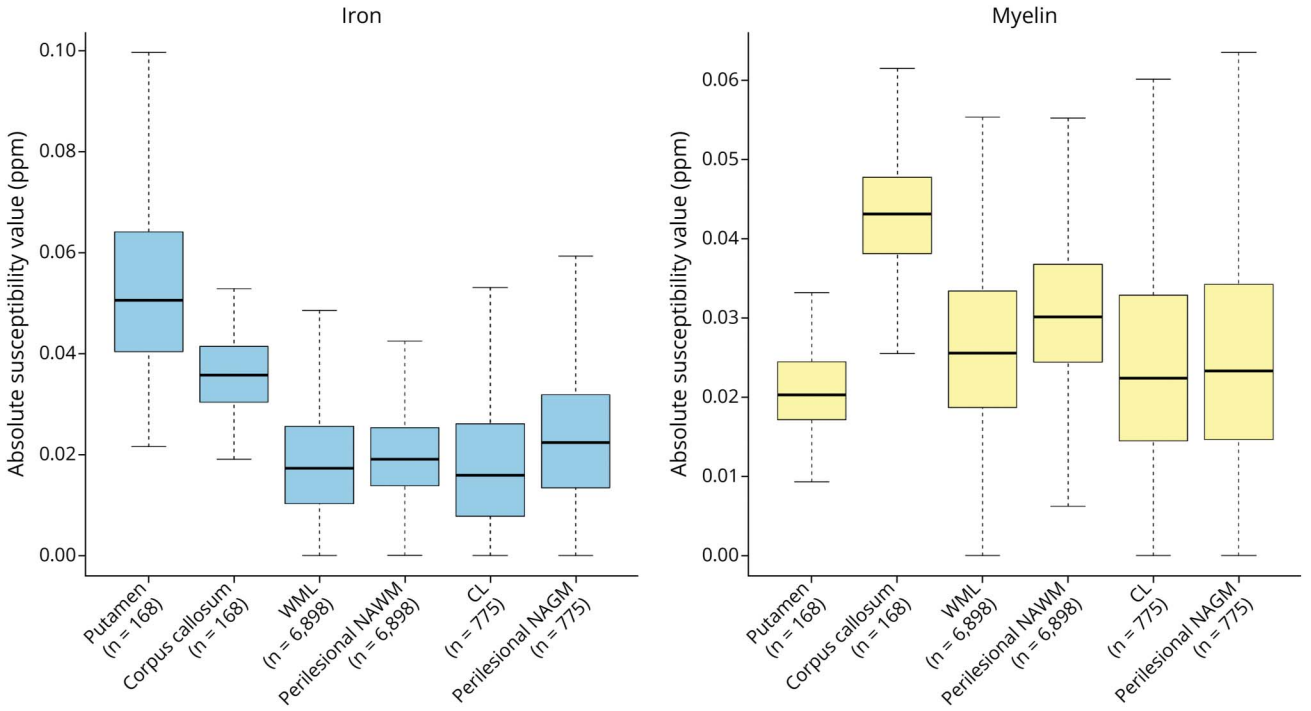

Absolute susceptibility values of iron (blue) and myelin (yellow) at baseline are displayed, in white matter and cortical lesions, as well as the perilesional normal appearing white and gray matter. In addition, the corpus callosum (as a referential region of interest with a high content of myelin) and the putamen (as a referential region of interest with a high content of iron) are displayed. CL = cortical lesions; NAGM = normal appearing gray matter; NAWM = normal appearing white matter; ppm = parts per million; WML = white matter lesion.

[IQR 0.40], $p < 0.001$ in Wilcoxon signed-rank test; $p = 0.001$ in linear mixed model adjusted for age, Figure 5, A and B).

In CLs, the median *absolute* susceptibility of myelin increased during follow-up (baseline median 0.023 [IQR 0.019], follow-up median 0.024 [IQR 0.17] ppm, $p = 0.03$, Wilcoxon signed-rank test), but this finding lost statistical significance when adjusting for age in a linear mixed model. The *absolute* content of iron remained stable between baseline (median 0.016 [IQR 0.018] ppm) and follow-up (0.015 [IQR 0.017] ppm). When considering the CLs *susceptibility index*, there was no change between baseline and follow-up for myelin, while the *susceptibility index* of iron increased over time (baseline median 0.730 [IQR 0.59], follow-up 0.739 [IQR 0.49], $p = 0.003$, Wilcoxon signed-rank test, Figure 5, C and D). However, the latter finding lost statistical significance after adjusting for age in a linear mixed model.

The *absolute* change of myelin between baseline and follow-up was larger in WMLs of patients with younger age ($p < 0.001$, $b = -5.111 \times 10^{-5}$, $aR^2 = 0.003$, linear regression model), lower EDSS ($p = 0.04$, $b = -2.352 \times 10^{-5}$, $aR^2 = 0.002$, linear regression model adjusted for age), and RRMS phenotype (RRMS median 0.003 [IQR 0.01] vs SPMS median 0.0004 [IQR 0.01], $p < 0.001$; RRMS vs PPMS median 0.002 [IQR 0.01] ppm, $p < 0.001$; both Wilcoxon signed-rank test), indicating a higher degree of remyelination in WMLs of those patients. In addition, changes of myelin in WMLs correlated with changes of EDSS during follow-up, with a higher degree of remyelination in patients with stable or improving EDSS ($p = 0.015$, $b = -6.686 \times 10^{-4}$, $aR^2 = 0.004$, linear regression model adjusted for age). Concerning the susceptibility of iron, we did not observe any correlation between disease characteristics and clinical changes during follow-up. The same was true for changes of myelin and iron in CLs.

When considering the median *susceptibility index* of all lesions per patient, we found that younger patients had a higher median increase in the index of myelin ($p = 0.02$, $b = -9.13 \times 10^{-4}$, $aR^2 = 0.047$) between baseline and follow-up. Furthermore, changes of myelin between baseline and follow-up correlated with the clinical improvement, as measured by EDSS ($p = 0.01$, $b = -1.6 \times 10^{-2}$, $aR^2 = 0.08$, linear regression model, adjusted for age, Figure 6). A similar tendency, however without reaching statistical significance, was found for CLs (data not shown). Although top improver (n = 12, 494 WMLs) and top progressor (n = 10, 415 WMLs) showed comparable proportions of lesions with increasing susceptibility index between baseline and follow-up (57% vs 53%), top improver exhibited a significantly larger median increment than top progressor (0.005 [IQR 0.005] vs 0.002 [0.002] ppm, $p = 0.005$, Wilcoxon signed-rank test, Figure 6).

Figure 5 Longitudinal Changes of Myelin and Iron in White Matter and Cortical Lesions

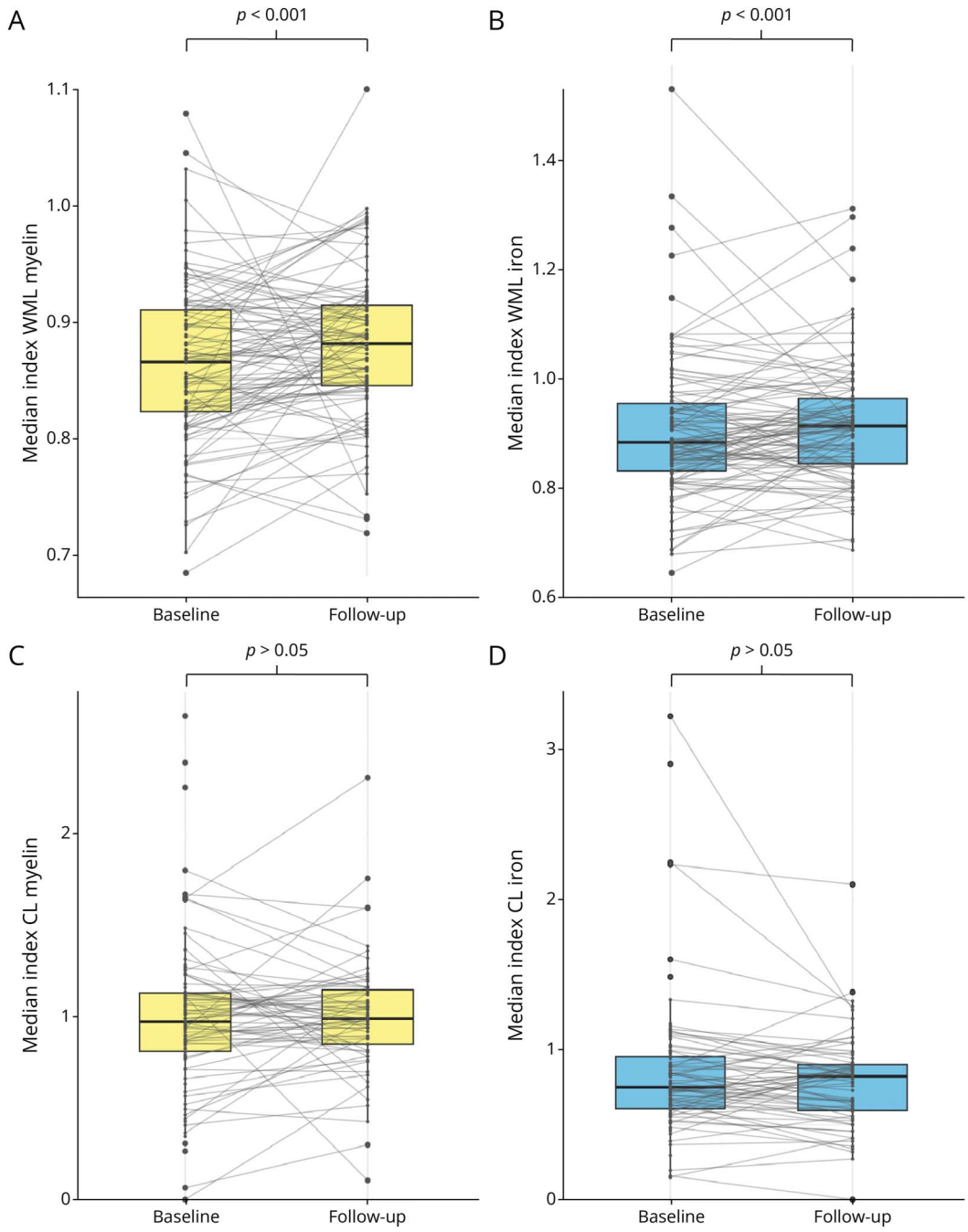

Susceptibility index for myelin in white matter lesions (A) and cortical lesions (C), as well as the susceptibility index for iron in white matter lesions (B) and cortical lesions (D) between baseline and 2-year follow-up. The *susceptibility index* describes the content of myelin (or iron, respectively) in the lesion, relative to the myelin (or iron, respectively) in perilesional normal appearing tissue. A susceptibility index of 1 indicates an equal susceptibility indicative of similar content of myelin (or iron, respectively) in lesional and perilesional tissue. One dot gives the median index of 1 patient. Diagonal lines connect the same patient between baseline and follow-up. *p* Values derive from linear mixed models adjusted for age. The figures indicate a significant increase of both myelin and iron in white matter lesions. Although there was a significant increase of iron in cortical lesions between baseline and follow-up, this finding lost its significance after adjustment for age. CL = cortical lesion; WML = white matter lesion.

Discussion

In this study, we implemented a novel mathematical model that leverages the frequency shift and transverse relaxation of MRI susceptibility signals (χ-separation)[18] to assess iron and myelin presence and changes in MS lesions. χ-separation showed comparable contents of myelin between patients with MS and healthy individuals in referential brain areas (putamen and corpus callosum), as well as a reduction of myelin in WMLs compared with the surrounding NAWM, but not in CLs compared with the NAGM. Furthermore, a longitudinal analysis of changes in χ-separation myelin maps showed a correlation between remyelination capacity—as quantified by an increase of myelin in WMLs

Figure 6 Changes in Myelin as Well as Clinical Changes Between Baseline and Follow-Up in White Matter Lesions

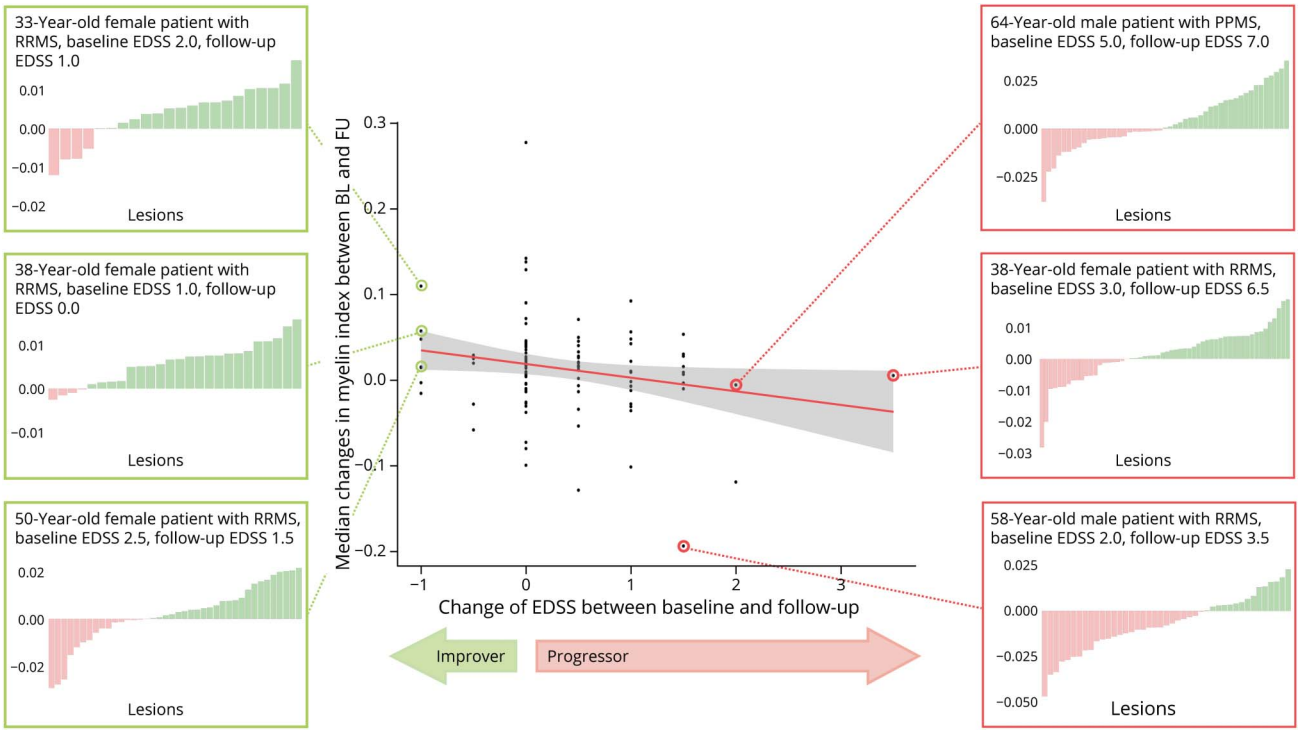

In the scatter plot, 1 dot represents 1 patient. The y-axis shows the median change in myelin *susceptibility index* between baseline and follow-up. The x-axis shows the change of EDSS between baseline and follow-up. The regression analysis indicates that patients with a greater increase of the median *susceptibility index* have larger clinical improvement. Bar charts show all lesions of selected patients with highest EDSS improvement (top improvers, green dots, left bar charts) and highest EDSS progression (top progressors, red dots, right bar charts), with demographic and clinical information. In the bar charts, red bars show lesions with a decrease of susceptibility on myelin-sensitive maps between baseline and follow-up (indicating demyelination), green bars show lesions with an increase of susceptibility on myelin-sensitive maps between baseline and follow-up (indicating remyelination). BL = baseline; EDSS = expanded disability status scale; FU = follow-up; PPMS = primary progressive multiple sclerosis; RRMS = relapsing-remitting multiple sclerosis; y/o = year old.

after 2 years—and clinical outcome—as measured by EDSS.

Our analysis of myelin in WMLs led to the expected result of significant reduction in the damaged area compared with the surrounding NAWM. Unexpectedly, in CLs, we did not see a difference in myelin between the lesion area and the surrounding NAGM. This could be attributed to either a milder myelin-related damage in focal lesions[36] or to diffuse demyelination in cortical areas without focal damage—as previously shown in histopathologic studies.[36,37] Nevertheless, it is also possible that partial volume effects may partly explain these findings because CLs identified on MP2RAGE are often quite small and the resolution of the applied MRI techniques might be insufficient for a detailed analysis of small structures. Against this latter explanation, however, speaks the fact that we observed a significantly lower level of iron in CLs compared with the NAGM. This finding is consistent with previous 7T QSM studies that suggested that iron loss dominates changes in the susceptibility contrast in CLs, rather than demyelination.[38]

Similar to previous studies,[5,39] we also found elevated iron in the putamen of patients with MS compared with healthy individuals. However, this finding lost statistical significance after adjustment for age. By contrast, in WMLs, the increase in iron between baseline and follow-up persisted after adjusting for age. These findings are intriguing, as iron accumulation has been described both as a physiologic age-related phenomenon[40] and pathologic process leading to neurodegeneration.[41] It has furthermore been attributed to a release by damaged oligodendrocytes,[42] which in turn is caused by microglial cells during inflammatory processes.[39] On the other hand, inflammation itself might lead to the production of reactive oxygen species and proinflammatory cytokines.[5,22] The fact that longitudinal increases of iron in WMLs persisted after age correction in our cohort provides an argument in favor of a pathology-related iron accumulation.

In a previous imaging-postmortem evaluation, QSM identified fully remyelinated lesions (shadow plaques) with a specificity of 100% but could not depict the dynamics of myelin reconstitution.[43] In this work, we have provided the first knowledge of how remyelination occurs over 2 years in patients with MS, in both CLs and WMLs. Our 2-year longitudinal analysis revealed in fact a broad range of changes in myelin, indicating significant variability of myelin loss and remyelination between and within participants. Of interest,

although this had been already reported in histologic studies,[44] we newly showed that signs of demyelination or remyelination correlated with clinical progression or improvement, as measured by EDSS. In line with previous PET studies using myelin-specific tracers,[7,8] signs of remyelination were particularly evident in patients with RRMS, younger age, and lower EDSS. Furthermore, our analysis of the most improving and most progressing patients supported the previously discussed distinction between good remyelinators and bad remyelinators,[7] with a larger increment of susceptibility in improving than in progressing patients, suggestive of a more pronounced remyelination in these patients (Figure 6). These results corroborate the ones obtained in previous PET studies[7] and provide new knowledge that it is possible to quantify clinically meaningful remyelination activity in vivo in MS patients without exposing patients to potentially harmful radiation.

Previous studies have shown that myelin water fraction (MWF)—a measure that is derived from T2 relaxometry experiments—provides sensitive and specific information about myelin content and integrity, both cross-sectionally[14,45] and longitudinally.[13,46] However, although the utility of WMF is widely indisputable, these studies have certain limitations: they did not directly correlate MRI findings with clinical outcomes,[13] were conducted on small cohorts,[13,45] or focused predominantly on gadolinium-enhancing lesions.[13] Furthermore, MWF is a fraction that is dependent on total water content; therefore, its values are influenced by the presence of active inflammation/edema; also, it has been suggested that MWF measurements are sensitive to iron influence, at least when some acquisition schemes are applied.[47,48] Therefore, since MWF is not solely influenced by myelin properties, it might be difficult to interpret its pathologic meaning in patients with MS. By exploiting the information derived by multiecho T2 and T2* experiments, χ-separation bypasses these limits and provides maps that are in theory not sensitive to global water content and iron. Nevertheless, also χ-separation suffers from inherent limitations: first, its dependency on myelin orientation may have influenced the *absolute* measurements in regions with variable myelin orientation. However, we anticipate that the *susceptibility index*, which assesses lesions relative to their local perilesional tissue with supposedly similar myelin orientation, may mitigate this effect. Second, although myelin and iron are recognized as primary susceptibility sources,[49] the potential contribution of local field inhomogeneities (static dephasing regime) and of other magnetic and paramagnetic trace elements, such as copper, manganese, or calcium, remains uncertain. Third, like all T2*-based image techniques, χ-separation is susceptible to reconstruction artifacts near areas prone to susceptibility effects. Furthermore, limitations of our study include the spatial resolution of the QSM map, that is probably not ideal to investigate CLs. We tried to avoid partial volume effects by setting a lesion size threshold, which we had to set lower for CLs compared with WMLs, to prevent exclusion of a substantial part of CLs. In addition, we could not assess lesion activity because we used MRI data that were obtained without gadolinium administration. This deliberate decision however was made to avoid potential interference with our susceptibility measurements.[50] Besides, as anticipated,[7] our exploratory analysis of WML heterogeneity (eMethods) revealed regional variations of demyelination or remyelination within lesions. Recognizing that our approach using the median susceptibility value for each lesion may not be ideal for capturing this heterogeneity, future studies should consider longitudinal assessment of voxel-wise susceptibility changes within lesions. In addition, given the predefined clinical follow-up of 2 years, we did not have the opportunity to confirm the EDSS at a third timepoint, but EDSS assessors were board-certified neurologists who underwent regular EDSS assessment trainings. In addition, similar to a previous study,[18] images with different spatial resolutions were used to apply the χ-separation method, which could have affected the estimation of myelin and iron values in small lesions. Future work should be devoted to develop clinical protocols including high-spatial and isotropic MEGRE and ME-T2 resolutions. Last but not least, our focus to investigate myelin and iron in MS lesions inherently precluded us from investigating equivalent lesional regions in healthy participants. Still, to ensure a meaningful comparison, we did not only report *absolute* values, but also the *susceptibility index*, which characterizes the lesional damage relative to the surrounding normal appearing tissue. In addition, we provided susceptibility measures of within-participant normal appearing tissues (specifically, corpus callosum and putamen) that are known for their content of myelin and iron, respectively, allowing us to validate our findings by aligning them with healthy individuals from our cohort and findings from previous studies.[22,23]

In conclusion, in this comprehensive cross-sectional and longitudinal study of a large cohort of patients with MS, we provided novel insights into the pathology of MS, shedding light on the changes of iron and myelin content in MS brains over time. Our results corroborate the utility of the χ-separation method in MS lesion characterization,[19] indicating the ability to precisely describe longitudinal myelin and iron changes on a lesional level. It therefore could serve as a valuable outcome measure in future clinical trials aiming at quantifying demyelination or remyelination, in a feasible acquisition time. Together, our findings not only enhance our understanding on the underlying mechanisms of MS pathology but also offer promising opportunities to facilitate the identification of effective remyelinating treatment strategies.

Study Funding

No targeted funding reported.

Disclosure

J. Müller has nothing to disclose about this work, he has received financial support by the Swiss National Science Foundation (grant no. P500PM_214230). P.-J. Lu reports no disclosures relevant to the manuscript. A. Cagol was

supported by EUROSTAR E!113682 HORIZON2020 and received speaker honoraria from Novartis. E. Ruberte reports no disclosures relevant to the manuscript. H.-G. Shin reports no disclosures relevant to the manuscript. M. Ocampo-Pineda reports no disclosures relevant to the manuscript. X. Chen reports no disclosures relevant to the manuscript. C. Tsagkas has nothing to disclose about this work, he has received financial support by the Swiss National Science Foundation (grant no. 320030_156860 and P500PM_206620), the National Multiple Sclerosis Society (grant no. FG-2107-38022), the Stiftung zur Förderung der gastroenterologischen und allgemeinen klinischen Forschung (application ID 02/2015), and the University of Basel (grant no. 3MS1020 and 3MS1049). M. Barakovic is an employee of Hays plc and a consultant for F. Hoffmann-La Roche Ltd. R. Galbusera reports no disclosures relevant to the manuscript. M. Weigel has received research funding by Biogen for developing spinal cord MRI. S.A. Schaedelin reports no disclosures relevant to the manuscript. Y. Wang received a grant from NIH and reports patents for QSM owned by Cornell University, owns stock/stock options in Medimagemetric. T.D. Nguyen reports no disclosures relevant to the manuscript. P. Spincemaille is an inventor of QSM-related patents issued to Cornell University and holds equity in Medimagemetric LLC, he is a paid consultant for Medimagemetric LLC. L. Kappos has received no personal compensation. His institutions (University Hospital Basel/Foundation Clinical Neuroimmunology and Neuroscience Basel) have received and used exclusively for research support: payments for steering committee and advisory board participation, consultancy services, and participation in educational activities from Actelion, Bayer, BMS, df-mp Molnia & Pohlmann, Celgene, Eli Lilly, EMD Serono, Genentech, Glaxo Smith Kline, Janssen, Japan Tobacco, Merck, MH Consulting, Minoryx, Novartis, F. Hoffmann-La Roche Ltd., Senda Biosciences Inc., Sanofi, Santhera, Shionogi BV, TG Therapeutics, and Wellmera, and license fees for Neurostatus-UHB products, grants from Novartis, Innosuisse, and Roche. J. Kuhle received speaker fees, research support, travel support, and/or served on advisory boards by Swiss MS Society, Swiss National Research Foundation (320030_189140/1), University of Basel, Progressive MS Alliance, Bayer, Biogen, Bristol Myers Squibb, Celgene, Merck, Novartis, Octave Bioscience, Roche, and Sanofi. J. Lee is an inventor of a χ-separation-related patent owned by Seoul National University and received financial support from National Research Foundation of Korea (NRF-2021R 1A2B5B03002783). C. Granziera, the University Hospital Basel (USB), as the employer of Cristina Granziera, has received the following fees which were used exclusively for research support (1) advisory board and consultancy fees from Actelion, Genzyme-Sanofi, Novartis, GeNeuro, and Roche; (2) speaker fees from Genzyme-Sanofi, Novartis, GeNeuro and Roche; and (3) research support from Siemens, GeNeuro, and Roche, she is supported by the Swiss National Science Foundation (SNSF) grant PP00P3_176984, the Stiftung zur Förderung der gastroenterologischen und allgemeinen klinischen Forschung and the EUROSTAR E!113682 HORIZON2020. Go to Neurology.org/N for full disclosures.

Publication History

Received by *Neurology* January 4, 2024. Accepted in final form May 20, 2024. Submitted and externally peer reviewed. The handling editor was Associate Editor Frederik Barkhof, MD, PhD, FRCR.

Appendix Authors

Name	Location	Contribution
Jannis Müller, MD, MSc	Translational Imaging in Neurology (ThINk) Basel, Department of Biomedical Engineering, Faculty of Medicine, and Neurologic Clinic and Policlinic, MS Center and Research Center for Clinical Neuroimmunology and Neuroscience Basel (RC2NB), University Hospital Basel and University of Basel, Switzerland	Drafting/revision of the manuscript for content, including medical writing for content; major role in the acquisition of data; study concept or design; analysis or interpretation of data
Po-Jui Lu, PhD	Translational Imaging in Neurology (ThINk) Basel, Department of Biomedical Engineering, Faculty of Medicine, and Neurologic Clinic and Policlinic, MS Center and Research Center for Clinical Neuroimmunology and Neuroscience Basel (RC2NB), University Hospital Basel and University of Basel, Switzerland	Drafting/revision of the manuscript for content, including medical writing for content; major role in the acquisition of data; analysis or interpretation of data
Alessandro Cagol, MD	Translational Imaging in Neurology (ThINk) Basel, Department of Biomedical Engineering, Faculty of Medicine, and Neurologic Clinic and Policlinic, MS Center and Research Center for Clinical Neuroimmunology and Neuroscience Basel (RC2NB), University Hospital Basel and University of Basel, Switzerland; Department of Health Sciences, University of Genova, Italy	Drafting/revision of the manuscript for content, including medical writing for content; major role in the acquisition of data; study concept or design; analysis or interpretation of data
Esther Ruberte, PhD	Translational Imaging in Neurology (ThINk) Basel, Department of Biomedical Engineering, Faculty of Medicine, and Neurologic Clinic and Policlinic, MS Center and Research Center for Clinical Neuroimmunology and Neuroscience Basel (RC2NB), University Hospital Basel and University of Basel, Switzerland	Major role in the acquisition of data; analysis or interpretation of data
Hyeong-Geol Shin, PhD	Laboratory for Imaging Science and Technology, Department of Electrical and Computer Engineering, Seoul National University, South Korea	Drafting/revision of the manuscript for content, including medical writing for content; major role in the acquisition of data

Continued

Appendix *(continued)*

Name	Location	Contribution
Mario Ocampo-Pineda, PhD	Translational Imaging in Neurology (ThINk) Basel, Department of Biomedical Engineering, Faculty of Medicine, and Neurologic Clinic and Policlinic, MS Center and Research Center for Clinical Neuroimmunology and Neuroscience Basel (RC2NB), University Hospital Basel and University of Basel, Switzerland	Drafting/revision of the manuscript for content, including medical writing for content; major role in the acquisition of data
Xinjie Chen, MD	Translational Imaging in Neurology (ThINk) Basel, Department of Biomedical Engineering, Faculty of Medicine, and Neurologic Clinic and Policlinic, MS Center and Research Center for Clinical Neuroimmunology and Neuroscience Basel (RC2NB), University Hospital Basel and University of Basel, Switzerland	Drafting/revision of the manuscript for content, including medical writing for content; major role in the acquisition of data
Charidimos Tsagkas, MD, PhD	Translational Imaging in Neurology (ThINk) Basel, Department of Biomedical Engineering, Faculty of Medicine, and Neurologic Clinic and Policlinic, MS Center and Research Center for Clinical Neuroimmunology and Neuroscience Basel (RC2NB), University Hospital Basel and University of Basel, Switzerland	Drafting/revision of the manuscript for content, including medical writing for content; major role in the acquisition of data
Muhamed Barakovic, PhD	Translational Imaging in Neurology (ThINk) Basel, Department of Biomedical Engineering, Faculty of Medicine, and Neurologic Clinic and Policlinic, MS Center and Research Center for Clinical Neuroimmunology and Neuroscience Basel (RC2NB), University Hospital Basel and University of Basel, Switzerland	Drafting/revision of the manuscript for content, including medical writing for content; major role in the acquisition of data
Riccardo Galbusera, MD	Translational Imaging in Neurology (ThINk) Basel, Department of Biomedical Engineering, Faculty of Medicine, and Neurologic Clinic and Policlinic, MS Center and Research Center for Clinical Neuroimmunology and Neuroscience Basel (RC2NB), University Hospital Basel and University of Basel, Switzerland	Drafting/revision of the manuscript for content, including medical writing for content; major role in the acquisition of data
Matthias Weigel, PhD	Translational Imaging in Neurology (ThINk) Basel, Department of Biomedical Engineering, Faculty of Medicine, and Neurologic Clinic and Policlinic, MS Center and Research Center for Clinical Neuroimmunology and Neuroscience Basel (RC2NB), University Hospital Basel and University of Basel; Division of Radiological Physics, Department of Radiology, University Hospital Basel, Switzerland	Drafting/revision of the manuscript for content, including medical writing for content; major role in the acquisition of data
Sabine A. Schaedelin, MSc	Translational Imaging in Neurology (ThINk) Basel, Department of Biomedical Engineering, Faculty of Medicine, University Hospital Basel and University of Basel; Department of Clinical Research, Clinical Trial Unit, University Hospital Basel, Basel, Switzerland	Drafting/revision of the manuscript for content, including medical writing for content; analysis or interpretation of data
Yi Wang, PhD	Department of Radiology, Weill Medical College of Cornell University, New York, NY	Drafting/revision of the manuscript for content, including medical writing for content
Thanh D. Nguyen, PhD	Department of Radiology, Weill Medical College of Cornell University, New York, NY	Drafting/revision of the manuscript for content, including medical writing for content
Pascal Spincemaille, PhD	Department of Radiology, Weill Medical College of Cornell University, New York, NY	Drafting/revision of the manuscript for content, including medical writing for content
Ludwig Kappos, MD	Translational Imaging in Neurology (ThINk) Basel, Department of Biomedical Engineering, Faculty of Medicine, and Neurologic Clinic and Policlinic, MS Center and Research Center for Clinical Neuroimmunology and Neuroscience Basel (RC2NB), University Hospital Basel and University of Basel, Switzerland	Drafting/revision of the manuscript for content, including medical writing for content; major role in the acquisition of data; study concept or design; analysis or interpretation of data
Jens Kuhle, MD, PhD	Department of Radiology, Weill Medical College of Cornell University, New York, NY	Drafting/revision of the manuscript for content, including medical writing for content; major role in the acquisition of data; analysis or interpretation of data
Jongho Lee, PhD	Laboratory for Imaging Science and Technology, Department of Electrical and Computer Engineering, Seoul National University, South Korea	Drafting/revision of the manuscript for content, including medical writing for content; major role in the acquisition of data; study concept or design; analysis or interpretation of data

Continued

Appendix *(continued)*

Name	Location	Contribution
Cristina Granziera, MD, PhD	Translational Imaging in Neurology (ThINk) Basel, Department of Biomedical Engineering, Faculty of Medicine, and Neurologic Clinic and Policlinic, MS Center and Research Center for Clinical Neuroimmunology and Neuroscience Basel (RC2NB), University Hospital Basel and University of Basel, Switzerland	Drafting/revision of the manuscript for content, including medical writing for content; major role in the acquisition of data; study concept or design; analysis or interpretation of data

References

1. Calabrese M, Magliozzi R, Ciccarelli O, Geurts JJ, Reynolds R, Martin R. Exploring the origins of grey matter damage in multiple sclerosis. *Nat Rev Neurosci*. 2015;16(3):147-158. doi:10.1038/nrn3900
2. Lubetzki C, Zalc B, Williams A, Stadelmann C, Stankoff B. Remyelination in multiple sclerosis: from basic science to clinical translation. *Lancet Neurol*. 2020;19(8):678-688. doi:10.1016/S1474-4422(20)30140-X
3. Neumann B, Segel M, Chalut KJ, Franklin RJ. Remyelination and ageing: reversing the ravages of time. *Mult Scler*. 2019;25(14):1835-1841. doi:10.1177/1352458519884006
4. Moller HE, Bossoni L, Connor JR, et al. Iron, myelin, and the brain: neuroimaging meets neurobiology. *Trends Neurosci*. 2019;42(6):384-401. doi:10.1016/j.tins.2019.03.009
5. Hametner S, Dal Bianco A, Trattnig S, Lassmann H. Iron related changes in MS lesions and their validity to characterize MS lesion types and dynamics with ultra-high field magnetic resonance imaging. *Brain Pathol*. 2018;28(5):743-749. doi:10.1111/bpa.12643
6. Ward RJ, Dexter DT, Crichton RR. Iron, neuroinflammation and neurodegeneration. *Int J Mol Sci*. 2022;23(13):7267. doi:10.3390/ijms23137267
7. Bodini B, Veronese M, Garcia-Lorenzo D, et al. Dynamic imaging of individual remyelination profiles in multiple sclerosis. *Ann Neurol*. 2016;79(5):726-738. doi:10.1002/ana.24620
8. Lazzarotto A, Tonietto M, Poirion E, et al. Clinically relevant profiles of myelin content changes in patients with multiple sclerosis: a multimodal and multi-compartment imaging study. *Mult Scler*. 2022;28(12):1881-1890. doi:10.1177/13524585221096975
9. Lee J, Shmueli K, Kang BT, et al. The contribution of myelin to magnetic susceptibility-weighted contrasts in high-field MRI of the brain. *Neuroimage*. 2012;59(4):3967-3975. doi:10.1016/j.neuroimage.2011.10.076
10. Langkammer C, Liu T, Khalil M, et al. Quantitative susceptibility mapping in multiple sclerosis. *Radiology*. 2013;267(2):551-559. doi:10.1148/radiol.12120707
11. Schmierer K, Scaravilli F, Altmann DR, Barker GJ, Miller DH. Magnetization transfer ratio and myelin in postmortem multiple sclerosis brain. *Ann Neurol*. 2004;56(3):407-415. doi:10.1002/ana.20202
12. Fujiyoshi K, Hikishima K, Nakahara J, et al. Application of q-space diffusion MRI for the visualization of white matter. *J Neurosci*. 2016;36(9):2796-2808. doi:10.1523/JNEUROSCI.1770-15.2016
13. Vargas WS, Monohan E, Pandya S, et al. Measuring longitudinal myelin water fraction in new multiple sclerosis lesions. *Neuroimage Clin*. 2015;9:369-375. doi:10.1016/j.nicl.2015.09.003
14. Rahmanzadeh R, Lu PJ, Barakovic M, et al. Myelin and axon pathology in multiple sclerosis assessed by myelin water and multi-shell diffusion imaging. *Brain*. 2021;144(6):1684-1696. doi:10.1093/brain/awab088
15. Granziera C, Wuerfel J, Barkhof F, et al. Quantitative magnetic resonance imaging towards clinical application in multiple sclerosis. *Brain*. 2021;144(5):1296-1311. doi:10.1093/brain/awab029
16. Deistung A, Schweser F, Reichenbach JR. Overview of quantitative susceptibility mapping. *NMR Biomed*. 2017;30(4):e3569. doi:10.1002/nbm.3569
17. Piredda GF, Hilbert T, Thiran JP, Kober T. Probing myelin content of the human brain with MRI: a review. *Magn Reson Med*. 2021;85(2):627-652. doi:10.1002/mrm.28509
18. Shin HG, Lee J, Yun YH, et al. χ-separation: magnetic susceptibility source separation toward iron and myelin mapping in the brain. *Neuroimage*. 2021;240:118371. doi:10.1016/j.neuroimage.2021.118371
19. Kim W, Shin HG, Lee H, et al. χ-separation imaging for diagnosis of multiple sclerosis versus neuromyelitis optica spectrum disorder. *Radiology*. 2023;307(1):e220941. doi:10.1148/radiol.220941
20. Thompson AJ, Banwell BL, Barkhof F, et al. Diagnosis of multiple sclerosis: 2017 revisions of the McDonald criteria. *Lancet Neurol*. 2018;17(2):162-173. doi:10.1016/S1474-4422(17)30470-2
21. Benkert P, Meier S, Schaedelin S, et al. Serum neurofilament light chain for individual prognostication of disease activity in people with multiple sclerosis: a retrospective modelling and validation study. *Lancet Neurol*. 2022;21(3):246-257. doi:10.1016/S1474-4422(22)00009-6
22. Haacke EM, Cheng NY, House MJ, et al. Imaging iron stores in the brain using magnetic resonance imaging. *Magn Reson Imaging*. 2005;23(1):1-25. doi:10.1016/j.mri.2004.10.001
23. Liu C, Li W, Johnson GA, Wu B. High-field (9.4 T) MRI of brain dysmyelination by quantitative mapping of magnetic susceptibility. *Neuroimage*. 2011;56(3):930-938. doi:10.1016/j.neuroimage.2011.02.024
24. Marques JP, Kober T, Krueger G, van der Zwaag W, Van de Moortele PF, Gruetter R. MP2RAGE, a self bias-field corrected sequence for improved segmentation and T1-mapping at high field. *Neuroimage*. 2010;49(2):1271-1281. doi:10.1016/j.neuroimage.2009.10.002
25. Nguyen TD, Deh K, Monohan E, et al. Feasibility and reproducibility of whole brain myelin water mapping in 4 minutes using fast acquisition with spiral trajectory and adiabatic T2prep (FAST-T2) at 3T. *Magn Reson Med*. 2016;76(2):456-465. doi:10.1002/mrm.25877
26. Karsa A, Shmueli K. SEGUE: a speedy region-growing algorithm for unwrapping estimated phase. *IEEE Trans Med Imaging*. 2019;38(6):1347-1357. doi:10.1109/TMI.2018.2884093
27. Wu B, Li W, Guidon A, Liu C. Whole brain susceptibility mapping using compressed sensing. *Magn Reson Med*. 2012;67(1):137-147. doi:10.1002/mrm.23000
28. Jenkinson M, Beckmann CF, Behrens TE, Woolrich MW, Smith SM. Fsl. *Neuroimage*. 2012;62(2):782-790. doi:10.1016/j.neuroimage.2011.09.015
29. La Rosa F, Abdulkadir A, Fartaria MJ, et al. Multiple sclerosis cortical and WM lesion segmentation at 3T MRI: a deep learning method based on FLAIR and MP2RAGE. *Neuroimage Clin*. 2020;27:102335. doi:10.1016/j.nicl.2020.102335
30. Fartaria MJ, Todea A, Kober T, et al. Partial volume-aware assessment of multiple sclerosis lesions. *Neuroimage Clin*. 2018;18:245-253. doi:10.1016/j.nicl.2018.01.011
31. Fartaria MJ, Kober T, Granziera C, Bach Cuadra M. Longitudinal analysis of white matter and cortical lesions in multiple sclerosis. *Neuroimage Clin*. 2019;23:101938. doi:10.1016/j.nicl.2019.101938
32. Yushkevich PA, Piven J, Hazlett HC, et al. User-guided 3D active contour segmentation of anatomical structures: significantly improved efficiency and reliability. *Neuroimage*. 2006;31(3):1116-1128. doi:10.1016/j.neuroimage.2006.01.015
33. Joshi S, Davis B, Jomier M, Gerig G. Unbiased diffeomorphic atlas construction for computational anatomy. *Neuroimage*. 2004;23(suppl 1):S151-S160. doi:10.1016/j.neuroimage.2004.07.068
34. R Core Team. *R: A Language and Environment for Statistical Computing*. R Foundation for Statistical Computing; 2014.
35. Khattar N, Triebswetter C, Kiely M, et al. Investigation of the association between cerebral iron content and myelin content in normative aging using quantitative magnetic resonance neuroimaging. *Neuroimage*. 2021;239:118267. doi:10.1016/j.neuroimage.2021.118267
36. Strijbis EMM, Kooi EJ, van der Valk P, Geurts JJG. Cortical remyelination is heterogeneous in multiple sclerosis. *J Neuropathol Exp Neurol*. 2017;76(5):390-401. doi:10.1093/jnen/nlx023
37. Haider L, Zrzavy T, Hametner S, et al. The topography of demyelination and neurodegeneration in the multiple sclerosis brain. *Brain*. 2016;139(pt 3):807-815. doi:10.1093/brain/awv398
38. Bian W, Tranvinh E, Tourdias T, et al. In vivo 7T MR quantitative susceptibility mapping reveals opposite susceptibility contrast between cortical and white matter lesions in multiple sclerosis. *Am J Neuroradiol*. 2016;37(10):1808-1815. doi:10.3174/ajnr.A4830
39. Bagnato F, Hametner S, Yao B, et al. Tracking iron in multiple sclerosis: a combined imaging and histopathological study at 7 Tesla. *Brain*. 2011;134(pt 12):3602-3615. doi:10.1093/brain/awr278
40. Todorich B, Pasquini JM, Garcia CI, Paez PM, Connor JR. Oligodendrocytes and myelination: the role of iron. *Glia*. 2009;57(5):467-478. doi:10.1002/glia.20784
41. Hallgren B, Sourander P. The effect of age on the non-haemin iron in the human brain. *J Neurochem*. 1958;3(1):41-51. doi:10.1111/j.1471-4159.1958.tb12607.x
42. Sun H, Walsh AJ, Lebel RM, et al. Validation of quantitative susceptibility mapping with Perls' iron staining for subcortical gray matter. *Neuroimage*. 2015;105:486-492. doi:10.1016/j.neuroimage.2014.11.010
43. Rahmanzadeh R, Galbusera R, Lu PJ, et al. A new advanced MRI biomarker for remyelinated lesions in multiple sclerosis. *Ann Neurol*. 2022;92(3):486-502. doi:10.1002/ana.26441
44. Huitema MJD, Strijbis EMM, Luchicchi A, et al. Myelin quantification in white matter pathology of progressive multiple sclerosis post-mortem brain samples: a new approach for quantifying remyelination. *Int J Mol Sci*. 2021;22(23):12634. doi:10.3390/ijms222312634
45. Kolind S, Matthews L, Johansen-Berg H, et al. Myelin water imaging reflects clinical variability in multiple sclerosis. *Neuroimage*. 2012;60(1):263-270. doi:10.1016/j.neuroimage.2011.11.070
46. Kitzler HH, Wahl H, Kuntke P, et al. Exploring in vivo lesion myelination dynamics: longitudinal myelin water imaging in early multiple sclerosis. *Neuroimage Clin*. 2022;36:103192. doi:10.1016/j.nicl.2022.103192
47. Laule C, Vavasour IM, Moore GR, et al. Water content and myelin water fraction in multiple sclerosis. A T2 relaxation study. *J Neurol*. 2004;251(3):284-293. doi:10.1007/s00415-004-0306-6
48. Birkl C, Birkl-Toeglhofer AM, Endmayr V, et al. The influence of brain iron on myelin water imaging. *Neuroimage*. 2019;199:545-552. doi:10.1016/j.neuroimage.2019.05.042
49. Langkammer C, Schweser F, Krebs N, et al. Quantitative susceptibility mapping (QSM) as a means to measure brain iron? A post mortem validation study. *Neuroimage*. 2012;62(3):1593-1599. doi:10.1016/j.neuroimage.2012.05.049
50. Swaminathan S. Gadolinium toxicity: iron and ferroportin as central targets. *Magn Reson Imaging*. 2016;34(10):1373-1376. doi:10.1016/j.mri.2016.08.016